Modeling a confined swirling coaxial jet

By C. A. Lin

1. Motivation and objectives

Swirling motion is often employed as a mechanism to further promote or control mixing between the fuel spray jet and the adjacent air and, in some occasions, to stabilize the combustion zone due to the presence of the swirl-induced central recirculation region. Since the central recirculation zone induced by the decay of swirl has profound effects on flame stabilization and mixing in combustion systems, a prior knowledge of the flow characteristics is beneficial during the design process.

To investigate the interaction of the air and fuel jet within a combustor, Johnson and Bennett (1981) conducted experiments of a non-reacting confined co-axial jet. Detailed measurements of the velocity and scalar fields were available to determine the turbulent transport processes within the flow. To examine the effects of swirling motion on the mixing characteristic, Roback and Johnson (1983) extended the previous non-swirling experiments to swirling co-axial jets. The results indicated that the peak momentum turbulent transport rates were approximately the same as those for the non-swirling flow condition. One distinct feature of the swirling case was the presence of the central recirculation zone, and the results indicated that the mixing for swirling flow was completed in one-third the length required for non-swirling flow.

In contrast to the traditional Reynolds averaged simulations, Akselvoll and Moin (1996) adopted a large eddy simulation technique to compute Johnson and Bennett's (1981) non-swirling co-axial jet case. Pierce and Moin (1998a,b) further extended the large eddy simulation to the swirling flow and validated their results with the experiments of Roback and Johnson (1983). Both the predicted velocity and scalar fields agreed well with the measurements. The Roback and Johnson case was also investigated by Brankovic *et al.* (1998), but within the Reynolds averaged equation framework. The results indicated that, although the velocity results compared favorably with the measurements, the scalar field was not reproduced correctly. The predicted results by Brankovic *et al.* showed an excessive level of mixing of the scalar field at the region bordering the central recirculation zone. It was indicated that unsteady effects, notably large-scale, low-frequency structures, may be responsible for the discrepancy in the predictions and measurements at this location.

The discrepancy of the predicted results between Pierce and Moin (1998a,b) and Brankovic *et al.* (1998) has motivated the present study to revisit the experimental study of Roback and Johnson computationally. The present computational framework is based on the Reynolds averaged equation approach, and the eddy-viscosity type turbulence models are adopted. Therefore, the objectives of the present study are to identify the causes of the discrepancies and to investigate the influences of grid density and turbulence modeling on the predicted results.

2. The computational model

2.1 The governing equations

The behavior of the flow is in general governed by the fundamental principles of classical mechanics expressing the conservation of mass, momentum, and passive scalar. The time-averaged equations for high-Reynolds-number flow may be described by the equations (in Cartesian tensor):

$$\frac{\partial(\rho U_i)}{\partial x_i} = 0$$

$$\frac{\partial(\rho U_i U_j)}{\partial x_j} = -\frac{\partial P}{\partial x_i} + \frac{\partial}{\partial x_j}[\mu_l(\frac{\partial U_i}{\partial x_j} + \frac{\partial U_j}{\partial x_i}) - \rho\overline{u_i u_j}]$$

$$\frac{\partial \rho U_j \Phi}{\partial x_j} = \frac{\partial}{\partial x_j}[\frac{\mu_l}{\sigma}\frac{\partial \Phi}{\partial x_j} - \rho\overline{u_j \phi}]$$

where $\overline{u_i u_j}$ and $\overline{u_j \phi}$ are the turbulent fluxes arising from the time-averaging process. μ_l and σ are the viscosity and Prandtl number, respectively. The tensorial form of the momentum equation represents the U, V, and rW momentum solved.

Within the framework of eddy-viscosity and adopting the Boussinesq approximation, the Reynolds stress and scalar flux are approximated as:

$$-\rho\overline{u_i u_j} = \mu_t(\frac{\partial U_i}{\partial x_j} + \frac{\partial U_j}{\partial x_i}) - \frac{2}{3}\delta_{ij}\rho k$$

$$-\rho\overline{u_j \phi} = \frac{\mu_t}{\sigma_t}\frac{\partial \Phi}{\partial x_j}$$

where μ_t and σ_t are turbulent viscosity and Prandtl number, respectively. The turbulent Prandtl number is assumed to be 0.9.

2.2 Turbulence models

In the present application, turbulence is described by the high-Reynolds-number $k-\epsilon$ eddy-viscosity model (Jones & Launder, 1972) and $k-\epsilon-v^2-f$ model (Durbin, 1995).

The $k-\epsilon$ model can be summarized as,

$$\mu_t = 0.09\rho\frac{k^2}{\epsilon}$$

$$\frac{\partial \rho U_j k}{\partial x_j} = \frac{\partial}{\partial x_j}(\mu_t\frac{\partial k}{\partial x_j}) - \rho\overline{u_i u_j}\frac{\partial U_i}{\partial x_j} - \rho\epsilon$$

$$\frac{\partial \rho U_j \epsilon}{\partial x_j} = \frac{\partial}{\partial x_j}(\frac{\mu_t}{1.3}\frac{\partial \epsilon}{\partial x_j}) + \frac{\epsilon}{k}(-1.44\rho\overline{u_i u_j}\frac{\partial U_i}{\partial x_j} - 1.92\rho\epsilon)$$

The $k-\epsilon-v^2-f$ model incorporates two additional equations f and $\overline{v^2}$ and is expressed as,

$$\mu_t = 0.19\rho\overline{v^2}T$$

$$\frac{\partial \rho U_j k}{\partial x_j} = \frac{\partial}{\partial x_j}(\mu_t \frac{\partial k}{\partial x_j}) - \rho\overline{u_i u_j}\frac{\partial U_i}{\partial x_j} - \rho\epsilon$$

$$\frac{\partial \rho U_j \epsilon}{\partial x_j} = \frac{\partial}{\partial x_j}(\frac{\mu_t}{1.3}\frac{\partial \epsilon}{\partial x_j}) + \frac{1}{T}(-C_{\epsilon 1}\rho\overline{u_i u_j}\frac{\partial U_i}{\partial x_j} - 1.9\rho\epsilon)$$

$$\frac{\partial \rho U_j \overline{v^2}}{\partial x_j} = \frac{\partial}{\partial x_j}(\mu_t \frac{\partial \overline{v^2}}{\partial x_j}) + \rho k f - \rho\frac{\overline{v^2}}{k}\epsilon$$

$$f = L^2\frac{\partial^2 f}{\partial x_j^2} - 0.3\frac{\overline{u_i u_j}}{k}\frac{\partial U_i}{\partial x_j} - (1-1.4)\frac{1}{T}(\frac{2}{3} - \frac{\overline{v^2}}{k})$$

$$C_{\epsilon 1} = 1.3 + \frac{0.25}{(1+(y/2\ell)^2)^4}$$

where y is the distance to the closest wall and,

$$T = max\left[\frac{k}{\epsilon}, 6(\frac{\nu}{\epsilon})^{1/2}\right], \quad L = 0.3\ell, \quad \ell = max\left[\frac{k^{3/2}}{\epsilon}, 70(\frac{\nu^3}{\epsilon})^{1/4}\right]$$

2.3 Numerical algorithm

This scheme solves discretized versions of all equations on a staggered finite-volume arrangement. The principle of mass-flux continuity is imposed indirectly via the solution of pressure-correction equations according to the SIMPLE algorithm (Patankar, 1980). The flow-property values at the volume faces contained in the convective fluxes which arise from the finite-volume integration process are approximated by the quadratic upstream-weighted interpolation scheme QUICK (Leonard, 1979).

The solution process consists of a sequential algorithm in which each of the sets of equations, in linearized form, is solved separately by application of an alternate-direction tri- or penta-diagonal line-implicit solver. Convergence was judged by monitoring the magnitude of the absolute residual sources of mass and momentum, normalized by the respective inlet fluxes. The solution was taken as having converged when all above residuals fell below 0.01%.

3. Geometry and boundary conditions

The geometry of the model combustor (Roback & Johnson, 1983) consists of an annular duct and a smaller center tube. Passive scalar is supplied through the center tube and the swirling flow is imposed on the annular duct. The two streams meet after a sudden expansion. The inlet Reynolds number based on the overall mass flow rate and the jet diameter is 80,300 and the swirl number is 0.41.

The inlet section of the computational domain is located before the expansion. Because no measured data were available, a fully developed profile was adopted. However, the prescription of inlet swirl profile for the annular duct was needed.

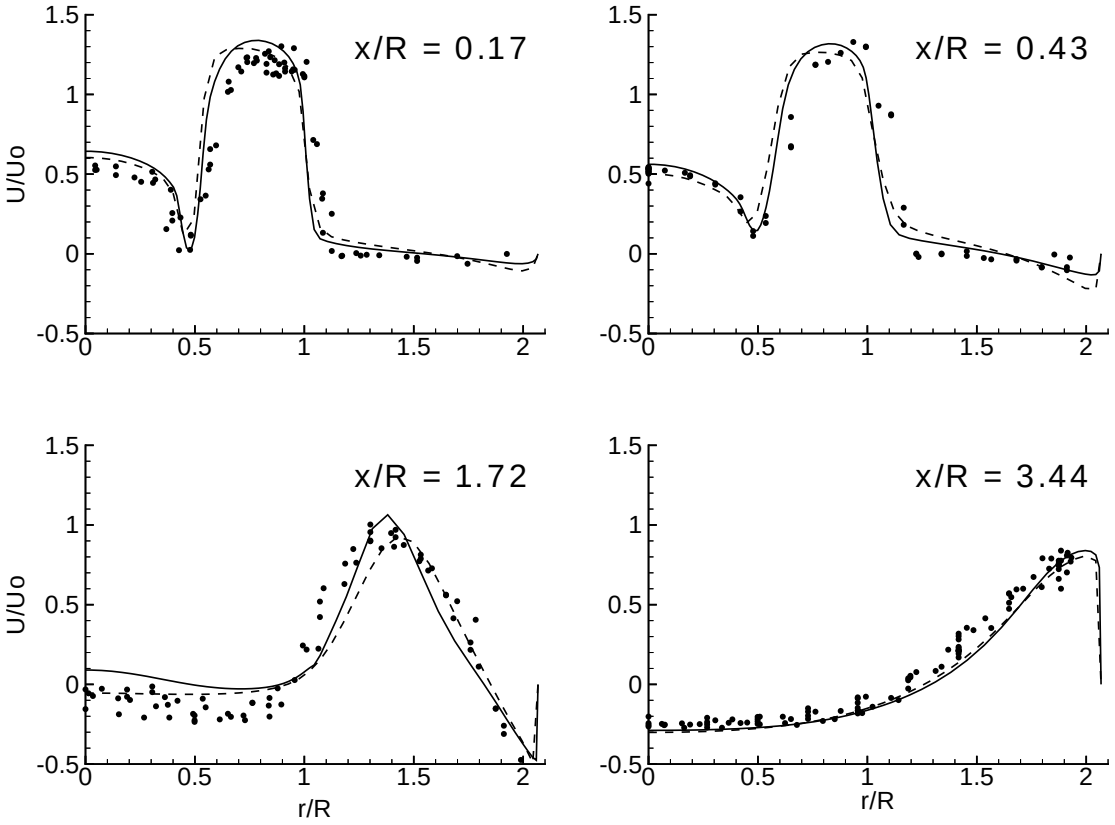

FIGURE 1. Effect of grid density on axial velocity distributions. Symbols: • , exp; ——— , k-ϵ 126x65; – – – – , k-ϵ 70x40.

The inlet swirl profile was obtained by applying a constant forcing function in the tangential momentum equation to generate the desired swirl level, a technique developed by Pierce and Moin (1998b).

The treatment at the axis of symmetry simply involved the prescription of zero-gradient conditions for all quantities except radial velocity, which was set to zero. Zero-streamwise-gradient conditions were prescribed along the computational outlet plane.

At the wall, the tangential velocity component U was assumed to vary logarithmically between the semi-viscous sub-layer, at $y_v^+ = 11.2$, and the first computational node lying in the region $30 < y^+ < 100$. The linear variation of the turbulent length scale, $L = \kappa y/C_\mu^{3/4}$, in the log-law region, together with $\epsilon = k^{3/2}/L$, and the invariant value $\epsilon = 2\mu_l k_v/(\rho y_v^2)$ in the viscous sub-layer, allowed the volume-averaged dissipation rate to be determined. This same L-variation was also used to prescribe explicitly the dissipation rate at the near-wall computational node, serving as the boundary condition for inner-field cells.

4. Results and discussions

The case computed was investigated experimentally by Roback and Johnson

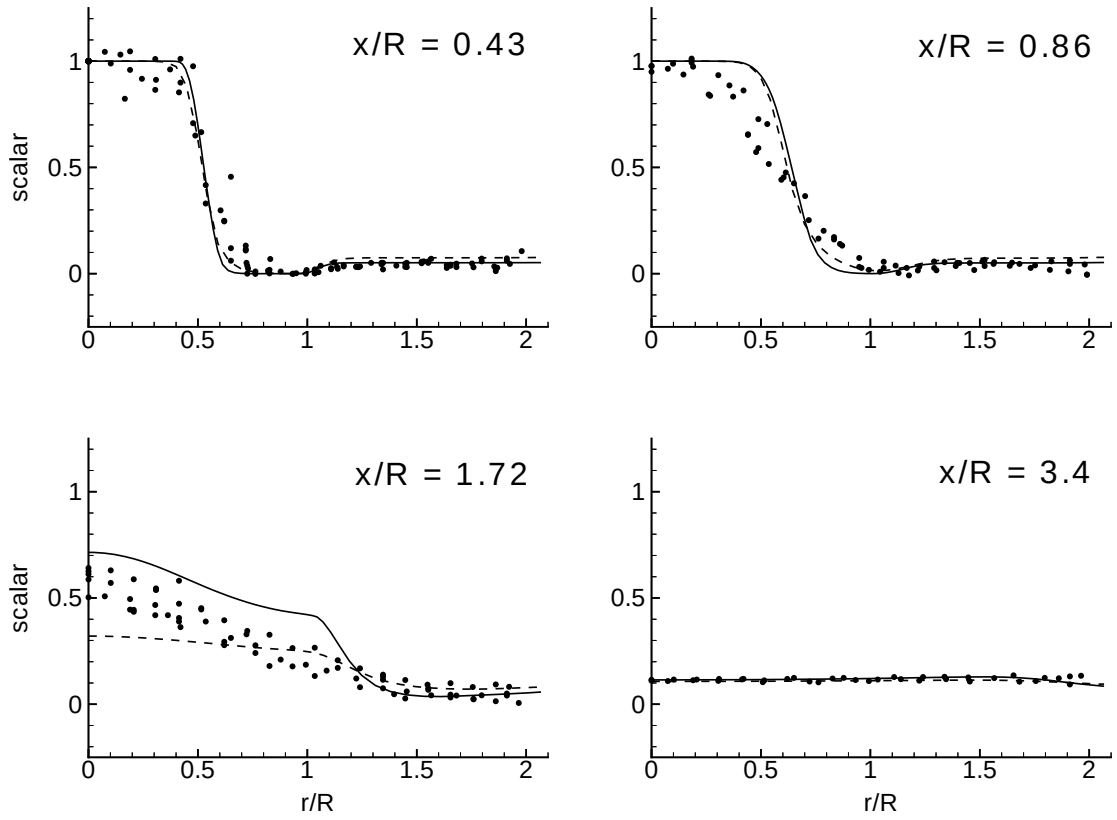

FIGURE 2. Effect of grid density on temperature distributions. Symbols: • , exp; ——— , k-ϵ 126x65; – – – – , k-ϵ 70x40.

(1983), where the swirl number and Reynolds number based on the inlet jet velocity are 0.41 and 80,300, respectively. This case was also investigated numerically using large eddy simulation (Pierce & Moin, 1998a); therefore, the predicted results will be contrasted with both measurements and LES results. Under highly swirling conditions it was generally recognized that the eddy-viscosity is not able to capture the strong swirl and turbulence interaction, and the Reynolds stress model is better in this situation (Lin *et al.*, 1996, Chen & Lin, 1998). However, for engineering computations the Reynolds stress transport models are expensive. In the present case, the swirl level is modest; therefore, it would be desirable to investigate the performance of the eddy viscosity models in this complex environment. The inclusion of the $k-\epsilon-\overline{v^2}f$ (v^2f) is motivated by the fact that it performed well in highly separated flow; however, few applications of the model were directed to swirling flows.

4.1 Effects of grid density

Before proceeding to the discussion of the predicted results, it will be beneficial to focus first on the effects of the grid density on the solutions. In the present computations, two meshes of sizes 70x40 and 126x65, which are nonuniform both in the x and y directions, were adopted to compute the flow. Initial tests on the

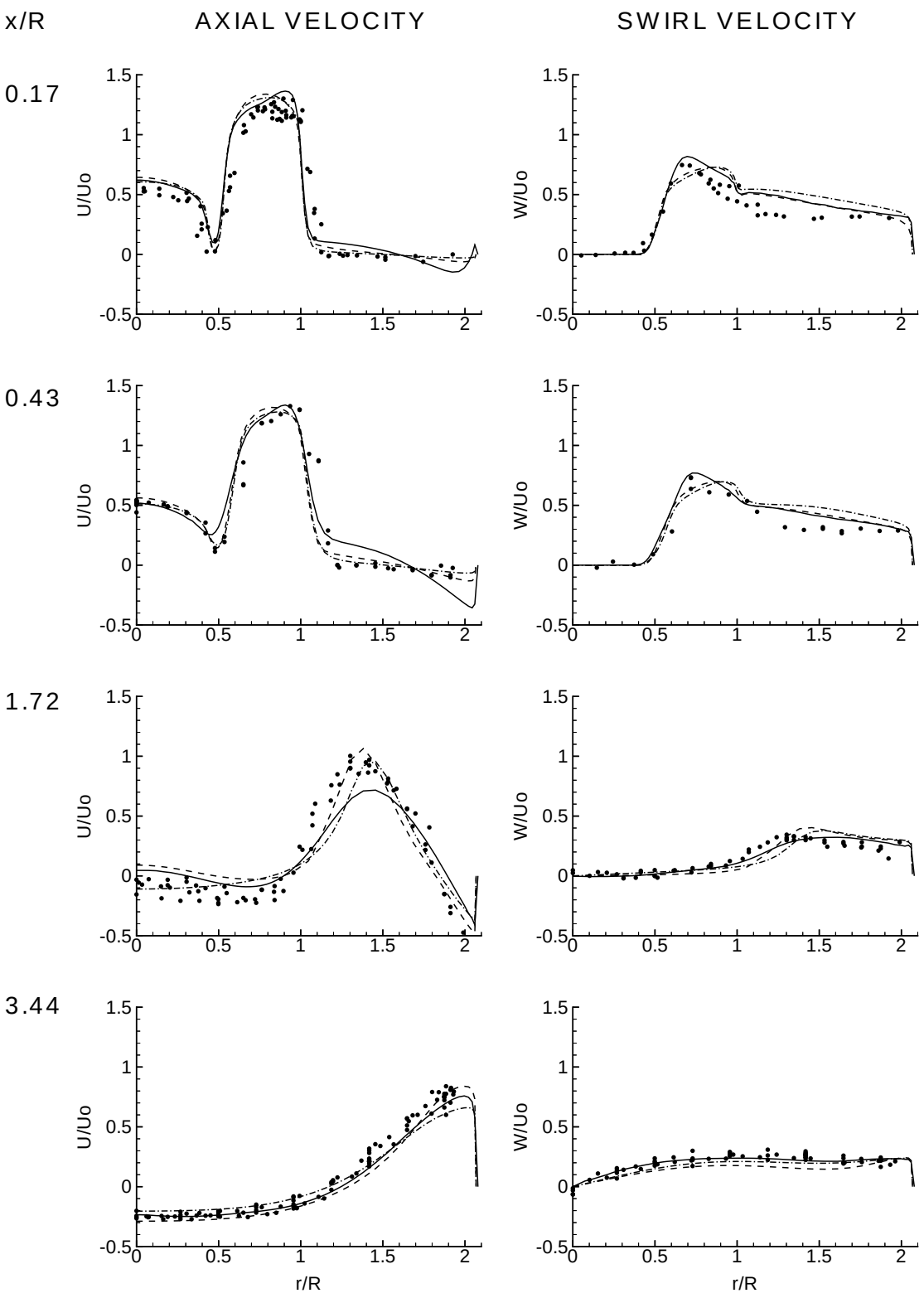

FIGURE 3. Predicted axial and tangential velocity profiles. Symbols: • , exp; ——— , LES; - - - - , k-ϵ; —·— , v^2f.

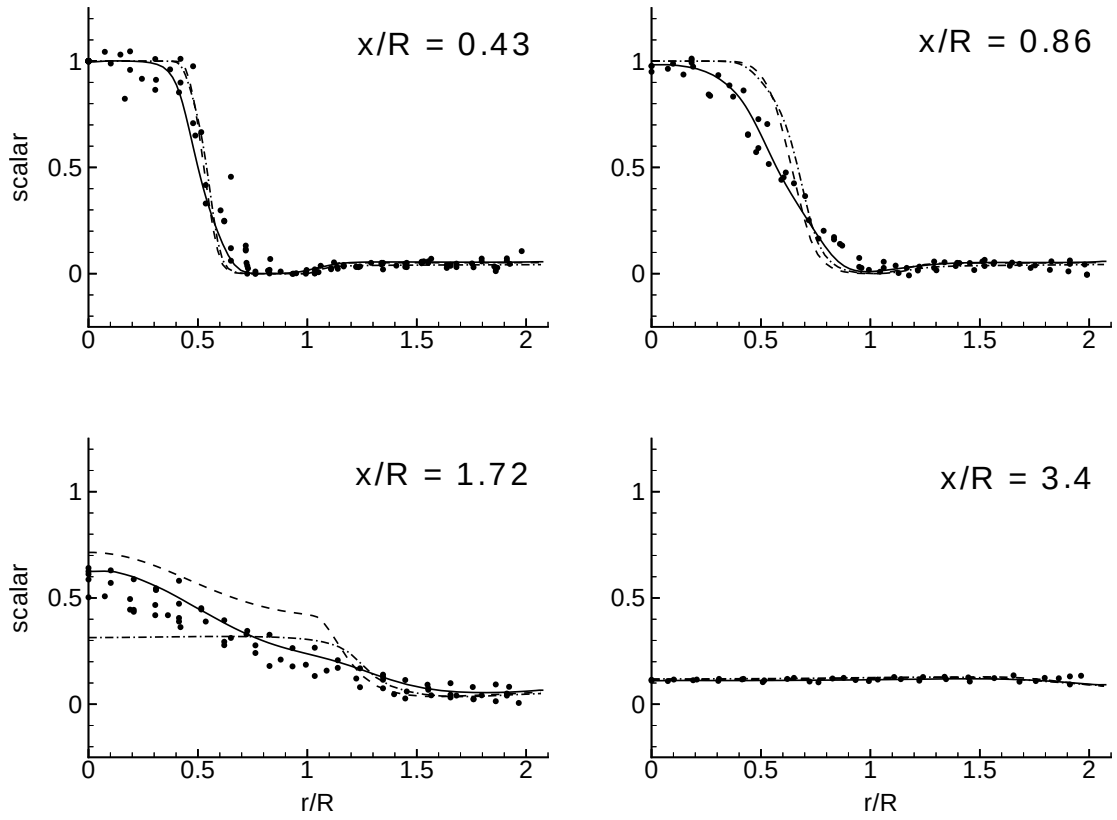

FIGURE 4. Predicted scalar field profiles. Symbols: • , exp; ——— , LES; – – – – , k-ϵ; —·— , v^2f.

influences of the convection schemes on the 126x65 grid revealed that the differences between the second order QUICK and the first order hybrid scheme were small.

The dominant features of the flow are the annular recirculation zone after the expansion and the extensive central recirculation zone due to the effect of the swirling co-axial jet. The presence of the center and corner recirculation zones is crucial to the stabilization of the combustion zone within the combustor. It is expected that the mixing within the recirculation is intense, resulting in an expectedly uniform scalar field.

The predicted axial velocity and scalar field at four selected locations are shown in Figs. 1 and 2. The fine grid produces a better resolution of the shear layer, as can be seen from Fig. 1. The coarse grid result, on the other hand, is shown to produce a higher level of diffusive transport, which causes the central jet to decay faster than the fine grid result. This is evidenced by reference to the axial velocity profile at $X/R = 1.72$, a location near the edge of the central recirculation zone. Although the differences of the predicted profiles at $X/R = 1.72$ is small, this small variation has profound influences on the predicted scalar field. This is because the coarse grid result shows the presence of the recirculation zone at this location, $X/R = 1.72$, where a more uniform scalar field is expected due to the elevated level of mixing.

By reference to Fig. 2, the difference of the two results can be seen to be marginal except at location $X/R = 1.72$. At this location, the coarse grid produces a uniform scalar field near the center line region while the fine grid shows a slightly steep variation of the passive scalar. As indicated earlier, this is related to the predicted strength of the central jet. For the fine grid result which shows a positive axial velocity at this location, a higher level of scalar field is transported downstream. For the coarse grid result which shows a negative axial velocity at this location, a lower level and uniform field of passive scalar is expected. It should be pointed out that the forward edge of the central recirculation zone is near the location $X/R = 1.72$. Therefore, the strength of the central jet has profound influences on the transport of the scalar field in this region. The non-physical diffusion tends to accelerate the decay of the central jet, and hence an earlier occurrence of the central recirculation zone. This results in a more uniform scalar field in this region. This argument is partly supported by the scalar field at $X/R = 3.4$. By reference to Fig. 1 at $X/R = 3.4$, it can be observed that the recirculation zone extends accross much of the width of the combustor. Therefore, a uniform scalar field is expected, and this is shown in Fig. 2 at $X/R = 3.4$.

Based on the above observation, the excessive level of mixing of the scalar field at the region bordering the central recirculation zone predicted by Brankovic *et al.* may be due to the insufficient grid density adopted in the solution domain.

4.2 Effects of turbulence modeling

Next, attention is focused on the effects of turbulence modeling on the predicted velocity and scalar fields. Figure 3 shows the predicted axial and tangential velocity profiles at four different axial locations. It can be seen that both the $k-\epsilon$ and v^2f models predict well the development of the mixing layer near r/R=0.5 before the central recirculation bubble, i.e. $X/R < 1.72$. It is interesting to see that the LES results show a slightly higher level of diffusive transport in the near field of the mixing layer.

The location of the central recirculation zone depends on the penetration strength of the central jet, and this can be clearly seen from the predicted axial velocity profiles at $X/R = 1.72$, shown in Fig. 3. The strength of the central jet predicted by the $k-\epsilon$ model is the strongest, and this is followed by the LES simulations. The v^2f prediction, on the other hand, is slightly diffusive, and hence a reverse flow is present along the centerline at this location, $X/R = 1.72$. The measurements indicate that part of the region near the centerline at $X/R = 1.72$ is within the central recirculation zone, and this seems to suggest that the v^2f model is correct. However, by reference to the scalar field at the same location, shown in Fig. 4, the v^2f model prediction is wrong. In contrast, the LES agrees well with measurements. The uniform scalar field predicted by the v^2f model is expected because the velocity field predicted indicates that this region is within the central recirculation zone where the mixing is good. This result is similar to the previous coarse grid $k-\epsilon$ predictions, and the predicted velocity field at this location is also similar as shown in Figs. 1 and 3 at $X/R = 1.72$. Therefore, the difference of the predicted scalar field at $X/R = 1.72$ is due to the predicted level of central jet penetration along the centerline.

Overall, the scalar field predicted by LES is better than the $k-\epsilon$ predictions even though the velocity field predicted by the latter model compares favorably with measurements. In strong contrast, the $k-\epsilon$ predictions show a reduced level of scalar mixing compared to the measured data. The cause of this is not clear, but it might be related to the defect of the constant Prandtl number approach adopted in the models. For example, by observing the predicted results at $X/R = 0.43$ and 0.86 in Fig. 4, it can be clearly seen that the adopted value of turbulent Prandtl number, 0.9, is too high. Other unsteady large scale motions, which are not accounted for by the present steady simulations, might have contributed to the enhanced mixing of the scalar field. The reduced level of mixing predicted by the $k-\epsilon$ model also causes the steep variation of the scalar profile around $r/R = 1.2$ at $X/R = 1.72$, as shown in Fig. 4.

REFERENCES

Akselvoll, K. & Moin, P. 1996 Large Eddy Simulation of Turbulent Confined Co-annular Jet. *J. Fluid Mech.* **315,** 387-411.

Brankovic, A., Ryder, Jr., R. C. & Syed, S. A. 1998 Mixing and Combustion Modeling for Gas Turbine Combustor using Unstructured CFD Technology. *AIAA-98-3854.*

Chen, J. C. & Lin, C. A. 1998 Modeling Strongly Swirling Flows with Second Moment Closure. *Int. J. Num. Methods in Fluids.* In press.

Durbin, P. A. 1995 Separated Flow Computations with the $k-\epsilon-v^2$ Model. *AIAA J.* **33,** 659-664.

Johnson, B. V. & Bennett J. C. 1981 Mass and Momentum Turbulent Transport Experiments with Confined Coaxial Jets. *NASA CR-165574.*

Jones, W. P. & Launder, B. E. 1972 The Prediction of Laminarization with a Two-Equation Model of Turbulence. *Int. J. Heat Mass Transfer.* **15,** 301-314.

Leonard, B. P. 1979 A Stable and Accurate Convective Modeling procedure Based on Quadratic Upstream Interpolation. *Comp. Meth. Appl. Mech. Eng.* **19,** 59-98.

Lin, C. H., Lin, C. A. & Chen, J. C. 1996 Modeling Influences of Inlet Swirl Profiles on Dump Combustor Flows. *AIAA J.* **34,** 2630-2632.

Patankar, S. V. 1980 *Numerical Heat Transfer and Fluid Flow.* Hemisphere Publishing Corporation.

Pierce, C. D. & Moin, P. 1998a Large Eddy Simulation of a Confined Coaxial Jet with Swirl and Heat Release. *AIAA 98-2892.* 29th AIAA Fluid Dynamics Conference, June 15-18, Albuquerque, NM.

Pierce, C. D. & Moin, P. 1998b Method for Generating Equilibrium Swirling Inflow Conditions. *AIAA J.* **36,** 1325-1327.

Roback, R. & Johnson, B. V. 1983 Mass and Momentum Turbulent Transport Experiments with Confined Swirling Coaxial Jets. *NASA CR-168252.*